interpretation, the non-positive value of β should be selected for the NCR case, and the role of incident and reflected waves for the NCR case should be reversed to that for the corresponding NNCR case. In conclusion, for reciprocal periodic TL structures based on the equivalent CCITL model, the non-negative and non-positive values of β should be selected for the NNCR and NCR cases respectively, as shown in Table 2 for physically and mathematically valid solutions of β. Note that Table 2 is obtained from Table 1 via the above conclusion.

4. CONCLUSIONS

This article shows the physical interpretation of NCRs of the equivalent CCITL model for terminated finite lossless reciprocal periodic TL structures, analyzed by using the CCITL theory. Generally, the equivalent CCITL model can provide both NNCR and NCR cases with appropriate propagation constant β. It is found that the propagation constant is the key parameter to physically interpret wave propagating phenomena for both NNCR and NCR cases; i.e., the non-negative and non-positive values of β are selected for the NNCR and NCR cases respectively as shown in Table 2. In addition, the roles of incident and reflected waves for the NNCR and corresponding NCR cases are reversed to each other to obtain correct physical interpretation.

ACKNOWLEDGMENTS

This work was supported by the Thailand Research Fund (TRF) and Commission on Higher Education (CHE) under the grant number MRG5380131.

REFERENCES

1. D. Torrungrueng and C. Thimaporn, A generalized ZY smith chart for solving nonreciprocal uniform transmission line problems, Microwave Opt Technol Lett 40 (2004), 57–61.
2. D. Torrungrueng and C. Thimaporn, Application of the T- chart for solving exponentially tapered lossless nonuniform transmission-line problems, Microwave Opt Technol Lett 45 (2005), 402–406.
3. D. Torrungrueng, C. Thimaporn, and N. Chamnandechakun, An application of the T-Chart for solving problems associated with terminated finite lossless periodic structures, Microwave Opt Technol Lett 47 (2005), 594–597.
4. A. Ishimaru, Electromagnetic wave propagation, radiation, and scattering, Prentice Hall, Upper Saddle River, NJ, 1991.
5. R.E. Collin, Foundations for microwave engineering, 2nd ed., McGraw Hill, New York, NY, 1992.
6. E. Takagi, Frequency dependence of bloch impedance in a periodic transmission line structure, Proc IEEE MTT-S Dig 2 (2001), 779–782.
7. R. S. Kshetrimayum and L. Zhu, Guided-wave characteristics of waveguide based periodic structures loaded with various FSS strip layers, IEEE Trans Antennas Propag 53 (2005), 120–124.
8. J. Gao and L Zhu, Characterization of infinite- and finite-extent coplanar waveguide metamaterials with varied left- and right-handed passbands, IEEE Microwave Wirel Compon Lett 15 (2005), 805–807.
9. S. Lamultree and D. Torrungrueng, On the characteristics of conjugately characteristic-impedance transmission lines with active characteristic impedance, Proceedings of Asia-Pacific Microwave Conference, Yokohoma, Japan, 2006, pp. 225–228.
10. D. Torrungrueng, S. Lamultree, C. Phongcharoenpanich, and M. Krairiksh, An in-depth analysis of reciprocal periodic structures of transmission lines, IET Trans Microwaves Antennas Propag 3 (2009), 591–600.
11. D.M. Pozar, Microwave engineering, 3rd ed., Wiley, NJ, 2005.

CALIBRATION METHODOLOGY FOR A 3D RADIATION PATTERN SET-UP OF PROBE-FED MILLIMETER-WAVE ANTENNAS

Diane Titz,[1] Mikko Kyrö,[2] Fabien Ferrero,[1] Sylvain Ranvier,[3] Cyril Luxey,[1,4] Patrice Brachat,[5] Gilles Jacquemod,[1] and Pertti Vainikainen[2]

[1] LEAT-CNRS, CREMANT, University of Nice-Sophia-Antipolis, 06560 Valbonne, France; Corresponding author: fabien.ferrero@unice.fr

[2] SMARAD/Department of Radio Science and Engineering, Aalto University, 00076 Aalto, Finland

[3] Belgian Institute for Space Aeronomy, B-1180 Bruxelles, Belgium

[4] Institut Universitaire de France (IUF), Maison des Universités, 75005 Paris, France

[5] CREMANT, Orange Labs, La Turbie, France

Received 1 August 2011

ABSTRACT: *In this article, we present a radiation pattern measurement setup for probe-fed millimeter-wave antennas and the associated calibration procedure. Compared with other existing facilities, our setup has one major innovation: it is composed of two rotating arms allowing measuring the radiated field of a probe-fed antenna over the quasi-3D sphere. The calibration challenges and issues encountered at 60 GHz are thoroughly described. We especially detail a specific calibration procedure to improve the accuracy of the measurements. To illustrate our methodology, the 3D radiation pattern measurement of a novel monopole-type antenna etched over a glass substrate is presented. Experimental results versus simulation results are compared.* © 2012 Wiley Periodicals, Inc. Microwave Opt Technol Lett 54:1183–1189, 2012; View this article online at wileyonlinelibrary.com. DOI 10.1002/mop.26795

Key words: *antenna measurements; radiation patterns; millimeter wave measurements; calibration proceduure*

1. INTRODUCTION

Millimeter waves are gaining a lot of interest for wireless personal area network applications, especially in the worldwide unlicensed band at 60 GHz [1]. Consequently, several standards defining these new possible applications have been recently issued [2–4]. Around this frequency, as the electromagnetic waves are strongly attenuated by the atmospheric oxygen absorption, high-gain antennas are needed to efficiently transmit electromagnetic waves over a few meters. Therefore, the 3D gain radiation pattern of these antennas has to be accurately measured. Some solutions exist and have already been reported. In Ref. 5, the authors present the measured maximum gain of a 60-GHz on-chip antenna without the associated radiation patterns. In Refs. 6 and 7, the two setups can only perform a radiation pattern measurement in limited cut-planes and a manual rotation of the receiving antenna is required. In Refs. 8 and 9, the presented setups can only achieve 2D radiation pattern cuts over a 180° scan. All these setups are able to characterize antennas fed by microelectronic probes. This is a really important feature because measuring connector-fed antennas at mm-wave frequencies often leads to inaccurate results as the necessary V-connector at 60 GHz is very often larger than the antenna itself [10]. So far, there is clearly a need to be able to measure the 3D radiation pattern of probe-fed antennas at millimeter-wave frequencies with a sufficient accuracy. Therefore, the calibration challenges and issues encountered in such measurements must be properly addressed for acceptable accuracy.

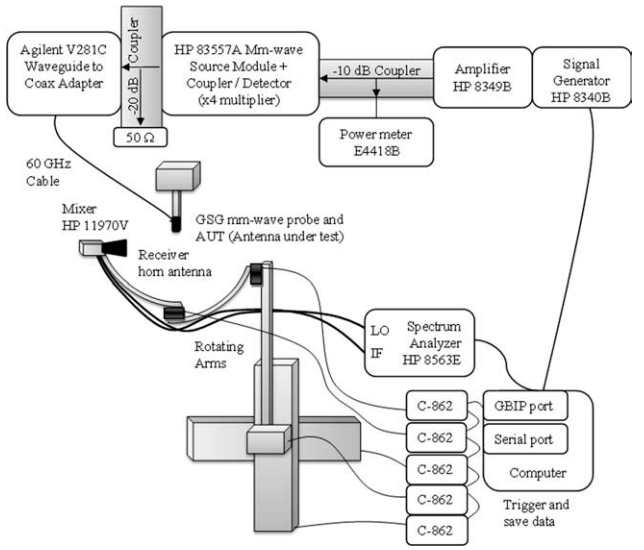

Figure 1 Schematic view of the radiation pattern setup

In this article, we propose to describe a setup able to measure the quasi-3D radiation pattern of probe-fed antennas in the 60-GHz frequency band [11]. We especially focus on the calibration methodology. First, we describe the mechanical and RF parts of the setup. We detail the two rotating arms allowing 3D scans around the antenna under test (AUT) and the special carrier of the AUT fabricated in rigid polyurethane material. This carrier offers the possibility to avoid any metallic chuck closely positioned under the AUT. Then, a thorough description of the calibration methodology is presented. The measurement and simulation results of a novel antenna etched over a glass substrate are also presented to validate our novel calibration methodology.

2. DESCRIPTION OF THE SETUP

A schematic view of the setup is presented in Figure 1. The RF blocks are placed on the upper part of the figure and the mechanical parts are described on the lower part.

2.1. RF Parts

A signal is generated by the HP 8340B synthesized generator at 15 GHz and amplified to 20 dBm by the HP 8349B amplifier. To control the power level of this signal and for calibration purpose, an Agilent E4418B power-meter connected through a 10 dB coupler is used after this amplification. Then, the signal is frequency multiplied four times with the help of an HP 83557A millimeter-wave source module and amplified to reach 12 dBm at 60 GHz. An Agilent V281A mm-wave-to-coax adapter allows conveying this signal to the microelectronic probe through a specific 60-GHz semi-rigid cable. A ground signal ground (GSG) microelectronic probe feeds the AUT (a Cascade Microtech i67-A-GSG-150 in the next measurement case). However, any other microelectronic probe can be used as a GSGSG. At the receiver side, an HP 11970V harmonic mixer is directly connected to a Flann 25240-20 horn antenna to down-convert the received 60-GHz signal. This direct attachment is indeed really important because the LO and IF low frequency signals, at respectively 4.3 GHz and 310 MHz, can be conveyed with low-cost flexible coaxial cables allowing the two rotating arms of the setup freely moving during the measurements. Because conveying low-frequency signals (4.3 GHz), this cable-arrangement especially helps to record the useful received signal with a better accuracy. The power level of the LO signal is monitored with an HP 8563E spectrum analyser. The generator and spectrum analyzer are controlled by a computer via GPIB and a custom-made Labview code. The frequency bandwidth of the setup is 50–75 GHz but it can be easily upgraded to measure antennas up to 110 GHz (new cables and/or waveguides and probes).

All the equipment used in transmission, from the signal generator to the mm-wave-to-coax adapter, can be replaced by an Agilent Power Network Analyzer (PNA) E8361A which enables the S11 measurement of the AUT and still the gain measurement. However, in this case the feeding signal of the AUT is lower than 0 dBm. A better dynamic range is obtained for the gain measurement in the previous configuration because the output power of the mm-wave source module is around 12 dBm. However, we have been able to alleviate this degradation by modifying the bandwidth of the IF filter of the spectrum analyzer used in the reception chain. Choosing a narrow filter-bandwidth or filter-resolution will enable to discriminate closely-spaced frequency signals. It will also reduce the noise level and therefore enable weaker signals to be recorded at the expense of the scanning rate of the analyzer spectrum. The narrower the bandwidth is, the slower the filter will respond to any signal changes and accordingly; the slower the spectrum analyzer will have to scan to ensure all the received signals are properly recorded. Another solution to speed-up again the measurement is to reduce the span around the center frequency in order to increase the scan rate of the spectrum analyzer.

2.2. Mechanical Parts

Two rotating arms are used to scan the quasi-3D sphere over the AUT, one of them holding both the receive horn antenna and the attached down-converter (mixer). The two rotations and the three translation axis of these arms are controlled by a computer. The distance between the receive horn and the AUT is chosen to be 20 cm. As the transmission distance is small, we are able to measure low-gain antennas. The far-field distance d_{far} can be computed from (1) where λ_0 is the free-space wavelength and D the largest dimension of the AUT.

$$d_{\text{far}} = \frac{2D^2}{\lambda_0} \tag{1}$$

Setting 20 cm and 60 GHz values in (1) allows claiming we are able to measure antennas with a largest dimension D equals to 2.2 cm. Compared with existing systems and more precisely to on-wafer setups [6], we do not use any metallic chuck to maintain the AUT. Therefore, no metallic parts are closely positioned to the AUT and strongly modify its radiation pattern. The setup presented in Ref. 7 is using a plastic support instead of a chuck but the measurement below the AUT cannot be performed. For each antenna, we always fabricate a specific foam holder which is screwed to a special carrier fabricated in rigid polyurethane material. The foam holder is chosen because its permittivity is close to one and does not introduce additional losses. However, for some antennas that need more rigid holders we can use FR4 knowing the fact that it will affect the radiation pattern. This special carrier is attached to a metallic 3D positioner classically used in a probe station. This blue carrier (Fig. 2) greatly helps in leaving free of any objects all the space around the AUT.

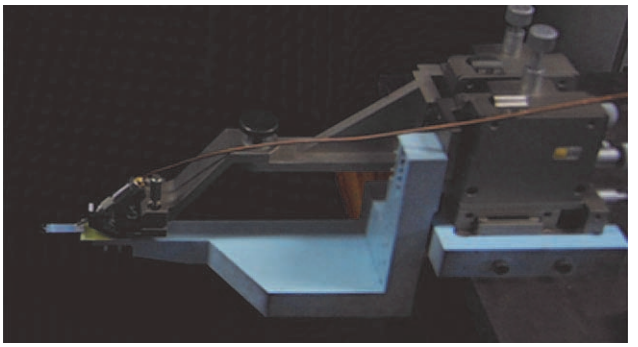

Figure 2 Picture of the 3D positioner (metal), the rigid polyurethane custom-made carrier (in blue) and the special FR4 holder of the on-glass substrate antenna. [Color figure can be viewed in the online issue, which is available at wileyonlinelibrary.com]

3. CALIBRATION

3.1. Mechanical Calibration Procedure

Several mechanical steps must be performed before starting the RF calibration. First, the AUT has to be positioned on its holder and the holder has to be screwed on the carrier. Then, a movable microscope is necessary to place the probe in-situ. Then, two laser pointers, which can fit into the center of a rotating arm, are used to accurately position the AUT at the center of the measurement sphere using the x, y, and z translation motors. Because the overall assembly of the two arms with the mixer and the horn antenna is a bit heavy (2 kg), a slight inflexion of the two arms is observed ($<2°$). However, we truly checked that no vibrations were happening during the measurements mainly because the two arms were designed in reinforced but lightweight aluminum. To avoid any electromagnetic reflexions and diffractions, these two aluminum arms are covered by thin-sheet absorbers.

3.2. RF Calibration Methodology

The calibration and the associated accuracy of such a setup are not trivial. In classic anechoic chambers, the RF calibration is usually achieved with two reference antennas, having a known realized gain. Designing a reference integrated antenna at these frequencies is quite challenging. So, we decided to implement a different sort of calibration. The first step is to monitor the output power of the amplifier and the mm-wave source module with a power meter (Fig. 3). We had to use two additional 10 dB couplers because indeed the two power sensors (E4413A and V8486A) are not able to absorb more than 20dBm without damages.

Then, we directly connect the 60-GHz cable to the receiving mixer using a waveguide-to-coax adapter instead of connecting this cable to the AUT via a probe (Fig. 4). The 20-dB coupler is still useful in that configuration to avoid any saturation of the mixer because the power delivered by the mm-wave source module is close to 12 dBm. With 12.5 dB lost in the cable and 0.5 dB lost in the adapters, the mixer experiences an input power close to -1 dBm, which is higher than its 1-dB compression point (-3 dBm).

This calibration is done for each polarization direction because we are forced to add two cables when we turn the receiving horn in order to measure the cross-polarization level.

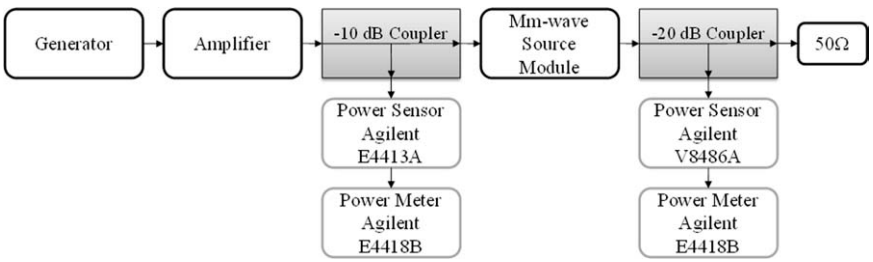

Figure 3 Schematic of the measurement of the output power of the amplifier and the output power of the mm-wave source module

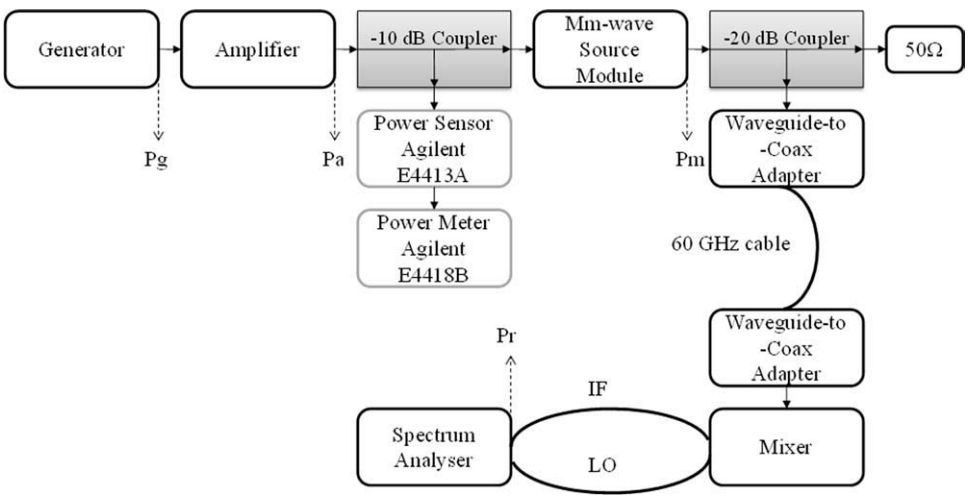

Figure 4 Schematic of the calibration method

TABLE 1 Losses and Accuracy of Each Term for the Computation of the Gain

Term	Value (in dB) @ 60 GHz	Accuracy (in dB) @ 60 GHz
Losses (Adapter)	−0.5	0.1
Losses (−20 dB coupler/coupled port)	−19.5	0.1
Losses (−20 dB coupler/direct port)	−0.33	0.1
PL	−53.81	0.2
Losses (Probe)	−0.5	0.1
Gr	19.6	0.2
TOTAL	16.04	0.8

The overall losses of the setup given in dB are then deduced from (2) using a simple transmission measurement knowing the output power of the amplifier (Pa) and the LO power (Pr) displayed on the spectrum analyzer. They can also be calculated between the output power of the mm-wave source module (Pm) and the LO power (Pr).

$$\begin{aligned}\text{Losses} = \text{Pr} - \text{Pa} = {} & \text{Losses (LO, IF cables)} + \text{Losses(Mixer)} \\ & + 2 \times \text{Losses (Adapter)} + \text{Losses(60 GHz cable)} \\ & + \text{Losses(}-\text{20 dB coupler/coupled port)} \\ & + \text{Losses(Mmwave source module)} \\ & + \text{Losses(}-\text{10dB coupler/direct port)} \end{aligned} \quad (2)$$

3.3. Computation of the Gain of an AUT

Knowing the overall losses computed during the calibration of the setup before every measurement, a very simple budget link is used to compute the gain of any AUT to be measured, for each polarization. This is done with the help of the simple Friis Equation given in dB in (3) where Gr and G are respectively the gains of the receive horn and the AUT (PL being the free-space loss defined by (4)). The gain of the horn (Gr) and the losses of the probe [Losses (Probe)] are given by the manufacturers of the corresponding devices and can be verified by dedicated measurements. The losses in the 20dB coupler and the adapters are extracted [Losses (−20 dB coupler/coupled port), Losses (−20 dB coupler/direct port), Losses (Adapter)] from its calibration and presented in Table 1.

$$\begin{aligned}\text{G} = {} & \text{Pr} - (\text{Pa} + \text{Gr} + \text{PL} + \text{Losses}) - \text{Losses (Probe)} \\ & + \text{Losses(Adapter)} - \text{Losses (}-\text{20dB coupler/direct port)} \\ & + \text{Losses (}-\text{20dB coupler/coupled port)} \end{aligned} \quad (3)$$

We can compute the path loss in dB from the distance between the AUT and the receive horn antenna, following (4).

$$\text{PL} = -20 \times \log\ 10\left(\frac{4\pi d}{\lambda_0}\right) \quad (4)$$

Then, the gain of the AUT can be extracted from (3) as the value of all the others quantity is known (Fig. 5).

3.4. Measurement Accuracy

To double-check the accuracy of our calibration, two calibrations are performed for a single measurement: one before the measurement and one afterwards. Those two measurements give us the repeatability of the computed losses [Losses in (3)]. However, for every term from the link budget (3), we need to know its uncertainty (Table 1). The uncertainty of the adapter and the 20-dB coupler has been measured with a 60-GHz PNA. The uncertainty of the computation of the path loss comes from the measurement of the distance between the transmitting and the receiving antennas. We estimated this distance to be 19.5 ± 0.5 cm, which leads to a path loss uncertainty of ± 0.2 dB. The losses of the probe and the gain of the horn antenna are from the datasheet of the manufacturers. The combination of all these numbers gives an overall gain uncertainty of ± 0.8 dB for both vertical and horizontal polarizations. At those frequencies, it is very tricky to improve this accuracy due to the difficulty to measure the exact losses of each part of the setup.

4. MEASUREMENT RESULTS

The radiation pattern measurement of a novel square monopole antenna etched on a glass substrate is presented to evaluate the consistency of the proposed calibration methodology and the

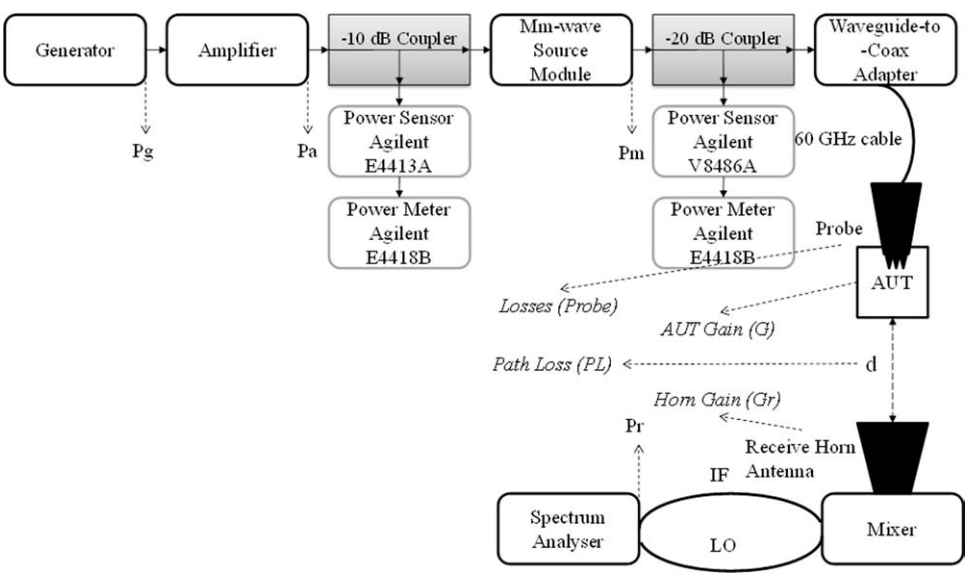

Figure 5 Schematic of the computation of the gain

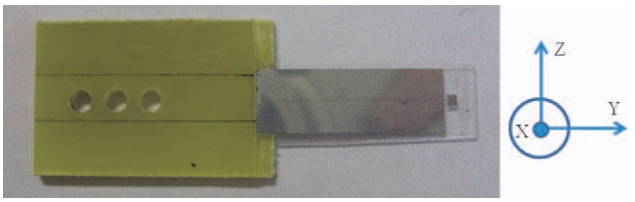

Figure 6 Picture of the square monopole etched on a glass substrate (right side). The special FR4 holder is seen on the left side of the picture. [Color figure can be viewed in the online issue, which is available at wileyonlinelibrary.com]

accuracy of the set-up. We especially performed a comparison between the 3D pattern measurements and the 3D pattern simulations achieved with the HFSS FEM-based 3-D full-wave electromagnetic solver. The antenna attached to its special FR4 holder is shown in Figure 6.

The monopole is fed by a 2-mm long coplanar line on which we directly place the tips of the probe for the measurement. Simulated and measured results of the total gain radiation pattern at 60 GHz in the three main planes are superposed in Figure 7. The feeding line is not de-embedded from the measurements and the simulation model includes this long line. First, we can see the setup limitations in terms of the possible angle to be measured. The full sphere is not covered due to the shape and the occupied space both by the probe and the holder. A 240° coverage is achievable in the *XY* and the *YZ* planes. A full 360° coverage is achievable in the *XZ* plane. The *XZ* plane is measured in two steps (see lower right corner of Fig. 7). First, the upper part of the plane is measured from 240 to 120°. Then, the lower part is measured from 60 to 300°. Consequently, the measured points between 60 and 120°; and 240 and 300° are measured twice with a 20 min delay. As shown in the lower right corner of Figure 7, the reproducibility of the measurement is quite remarkable. A very good agreement is seen between the simulated and the measured data. In the *XY* horizontal plane, the measurement is very close to the simulation especially between 240 and 330°. In the *YZ* vertical plane, the shaky simulated radiation pattern is validated by our measurement. Those simulated and measured ripples are attributed to the long feeding line and are not caused by the probe or the positioned (both not taken into account in the simulation model). In the *XZ* vertical plane, the measurement fits the ±0.8 dB precision for angles between 30° and 140°; and 220 and 325°. In this plane, the maximum measured gain is equal to 3 dBi compared with a 1.5 dBi simulated gain for $\theta = 94°$. In all these three planes, the simulated and measured gains are in a quite good agreement for most of the angles dealing with the ± 0.8 dB accuracy of the calibration methodology: especially 80% of the measured points belong to this accuracy range. Simulated and measured 3D plots are given in Figure 8 (dB scale). The shape, maximum and minimum of the two plots are indeed the same. The maximum measured gain is equal to 3.64 dBi in the direction $(\varphi, \theta)=(22°, 90°)$ compared with a 3.66 dBi simulated gain for $(\varphi, \theta)=(20°, 92°)$. To emphasize the

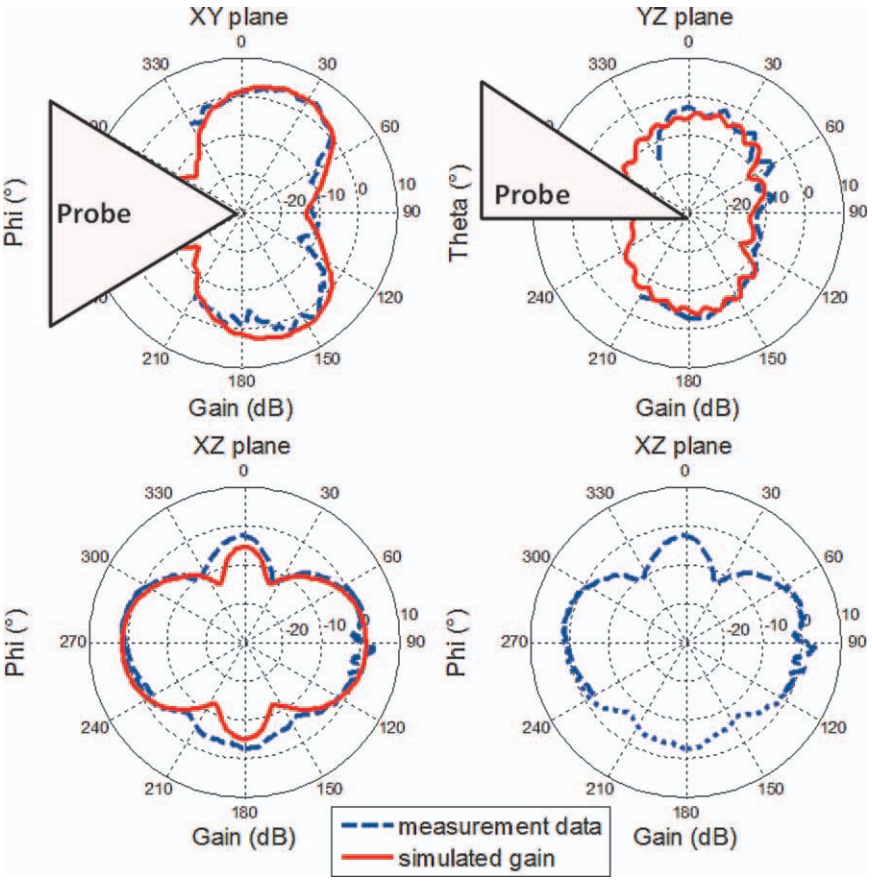

Figure 7 Simulation and measurement of the total gain radiation pattern of the antenna in three principal planes. The measurement in the XZ plane is plot alone in one of the graphs for a better understanding (lower right side). [Color figure can be viewed in the online issue, which is available at wileyonlinelibrary.com]

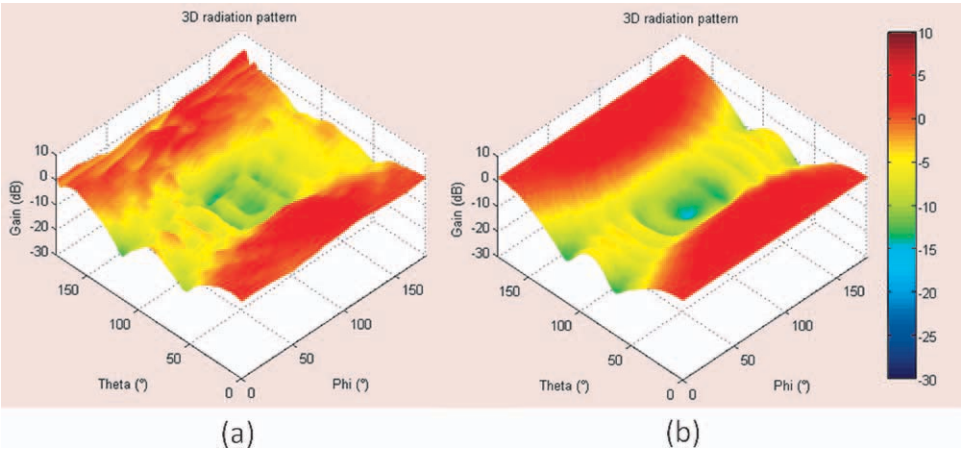

Figure 8 (a) Measurement and (b) simulation of the 3D gain radiation pattern. [Color figure can be viewed in the online issue, which is available at wileyonlinelibrary.com]

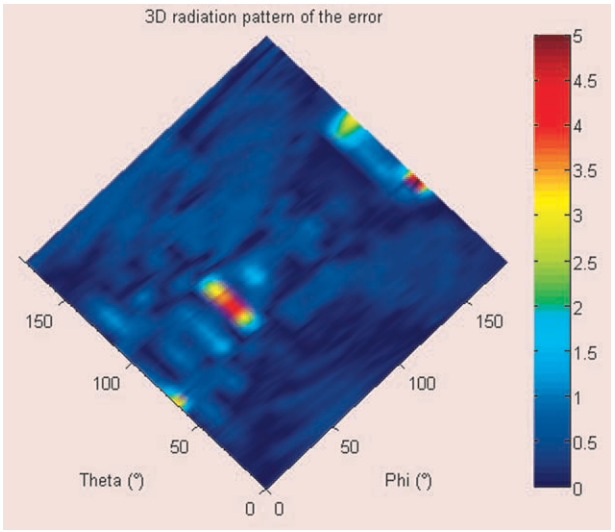

Figure 9 Error in % between the measured gain and the simulated gain in 3D. [Color figure can be viewed in the online issue, which is available at wileyonlinelibrary.com]

fact that we have a very good match in all the planes, we have plot the error in percentages between the simulated and measured patterns versus Phi and Theta angles (Fig. 9) following (5). The error is found to be lower than 5% in all the angles of the quasi-3D sphere. Several other antennas were measured using this measurement setup proving its ability, accuracy, and the validity of the calibration procedure [11–17].

$$\text{Error} = \left|\frac{\text{Simulated\_gain} - \text{Measured\_gain}}{\text{Simulated\_gain}}\right| \times 100 \qquad (5)$$

5. CONCLUSIONS

In this article, we presented a 3D radiation pattern measurement setup for probe-fed antennas. The setup allows measuring the quasi-3D radiation pattern with the help of two motorized arms. We especially focused on the calibration methodology. The total gain radiation pattern of a square monopole was presented as an example of the capabilities and the accuracy of the setup. We demonstrated a very good agreement between the simulated and measured results and an overall accuracy of ± 0.8 dB over the quasi-3D sphere.

ACKNOWLEDGMENTS

The authors would like to thank the CIMPACA Design Platform, the COST iC0603 and Orange Labs for their support.

REFERENCES

1. P. Smulders, Exploring the 60 GHz band for local wireless multimedia access: Prospects and future direction, IEEE Commun Mag 40 (2002), 140–147.
2. IEEE 802.15 WPAN Task Groups 3c, IEEE Standard 802, 2005.
3. IEEE 802.11 Task Groups ad, IEEE Standard 802, 2009.
4. ECMA-387 Standard, 2008. Available at: http://www.ecma-international.org/publications/files/ECMA-ST/ECMA-387.pdf
5. S.-S. Hsu, K-C. Wei, C-Y. Hsu, and H. Ru-Chuang, A 60-GHz millimeter-wave CPW-fed yagi antenna fabricated by using 0.18 μm CMOS technology, IEEE Elecron Device Lett 29 (2008), 625–627.
6. J.A.G. Akkermans, R. van Dijk, and M.H.A.J. Herben, Millimeter-wave antenna measurement, 37th EuMc, Munich, Germany, 2007, pp. 83–86.
7. R. Pilard, S. Montusclat, D. Gloria, F. Le Pennec, and C. Person, Dedicated measurement setup for millimetre-wave silicon integrated antennas: BiCMOS and CMOS high resistivity SOI process characterization, European Conference on Antennas and Propagation Eucap 2009, Berlin, Germany, pp. 2447–2451, 23–27 March 2009.
8. T. Zwick, D. Liu, and B.P. Gaucher, Broadband planar superstrate antenna for integrated millimeterwave transceivers, IEEE Trans Antennas Propag 54 (2006), 2790–2796.
9. J. Lantéri, L. Dussopt, R. Pilard, D. Gloria, S.D. Yamamoto, A. Cathelin, and H. Hezzeddine, 60 GHz antennas in HTCC and glass technology, European Conference on Antennas and Propagation, Eucap 2010, Barcelona, Spain, pp. 1–4, April 2010.
10. S. Ranvier, M. Kyro, C. Icheln, C. Luxey, R. Staraj, and P. Vainikainen, Compact 3-D on-wafer radiation pattern measurement system for 60 GHz antennas, Microwave Opt Technol Lett 51 (2009), 319–324.
11. D. Titz, M. Kyrö, F. Ben Abdeljelil, C. Luxey, G. Jacquemod, and P. Vainikainen, Radiation pattern measurement set-up for 60 GHz on-chip antennas, Antennas and Propagation Conference (LAPC) 2010, Loughborough, UK, pp. 533–536, 8–9 Nov. 2010.

12. D. Titz, F. Ben Abdeljelil, C. Luxey, and G. Jacquemod, Co-design of integrated antennas and CMOS switches for future indoor personal networks at 60 GHz, Antennas and Propagation Society International Symposium (APSURSI) 2010, Toronto, Canada, pp. 1–4, 11–17 July, 2010.
13. D. Titz, M. Kyrö, F. Ben Abdeljelil, C. Luxey, G. Jacquemod, and P. Vainikainen, Design and measurement of a dipole-antenna on a 130 nm CMOS substrate for 60 GHz communications, International Conference on Applied Electromagnetics and Communications (ICECom) 2010, Dubrovnik, Croatia, pp. 1–4, 20–23 September 2010.
14. C. Oikonomopoulos-Zachos, D. Titz, M. Martinez-Vazquez, F. Ferrero, C. Luxey, and G. Jacquemod, Accurate characterization of a 60 GHz antenna on LTCC substrate, European Conference on Antennas and Propagation (EuCAP) 2011, Rome, Italy, pp. 3117–3121, 11–15 April 2011.
15. D. Titz, A. Lamminen, M. Kyrö, F. Ferrero, C. Luxey, J. Säily, G. Jacquemod, and P. Vainikainen, 3D radiation pattern measurement of LTCC antennas at 60 GHz, 4th Global Symposium on Millimeter Waves, Espoo, Finland, May 2010.
16. D. Titz, R. Pilard, F. Ferrero, F. Gianesello, D. Gloria, C. Luxey, P. Brachat, and G. Jacquemod, 60 GHz antenna integrated on high resistivity silicon technologies targeting WHDMI applications, Radio Frequency Integrated Circuits Symposium, RFIC 2009, Baltimore, pp. 355–358, 5–7 June 2011.
17. D. Titz, F. Ferrero, C. Luxey, and G. Jacquemod, A novel fully-automatic 3D radiation pattern measurement setup for 60 GHz probe-fed antennas, Antennas and Propagation Society International Symposium APSURSI 2011, Spokane, USA, July 2011.

SMALL-SIZE LTE/WWAN COUPLED-FED LOOP ANTENNA WITH BAND-STOP MATCHING CIRCUIT FOR TABLET COMPUTER

Kin-Lu Wong and Tsung-Ju Wu
Department of Electrical Engineering, National Sun Yat-Sen University, Kaohsiung 804, Taiwan; Corresponding author: wongkl@ema.ee.nsysu.edu.tw

Received 11 July 2011

ABSTRACT: *By combining the use of a coupling feed and a band-stop matching circuit, the proposed small-size loop antenna for the tablet computer application can operate at its quarter-wavelength mode as the lowest resonant mode and provide two wide operating bands (704–960 and 1710–2690 MHz) to cover the eight-band LTE/WWAN operation (LTE700/GSM850/900 and GSM1800/1900/UMTS/LTE2300/2500 bands). The loop antenna comprises a T-shape radiating feed, a coupled shorted strip, an antenna ground, and a band-stop matching circuit on the antenna ground. The antenna's metal pattern includes a printed pattern on a thin FR4 substrate of planar size 10 × 55 mm^2 and a metal strip of size 4 × 55 mm^2 formed a part of the coupled shorted strip and connected orthogonally to the printed pattern. The antenna's occupied volume and the required length of 55 mm along the top edge of the display ground are both the smallest among the internal LTE/WWAN antenna for the tablet or laptop computers that have been reported for the present. Detailed operating principle of the proposed antenna including the effects of the coupling feed using the T-shape radiating feed and the band-stop matching circuit for bandwidth enhancement is discussed.* © 2012 Wiley Periodicals, Inc. Microwave Opt Technol Lett 54:1189–1193, 2012; View this article online at wileyonlinelibrary.com. DOI 10.1002/mop.26765

Key words: *mobile antennas; tablet computer antennas; WWAN antennas; LTE antennas; band-stop matching circuit*

1. INTRODUCTION

To cover the existing mobile communication systems for the laptop or tablet computer applications, which mainly include the eight-band LTE/WWAN operation in the 704–960 and 1710–2690 MHz bands, several internal antennas have been reported [1–4]. To provide two wide operating bands for the LTE/WWAN operation, these reported internal antennas are required to occupy a volume of 4 × 10 × 80 mm^3 [1], 4 × 12 × 70 mm^3 [2], 4 × 10 × 70 mm^3 [3], and 4 × 10 × 85 mm^3 [4]. That is, the reported internal LTE/WWAN antennas require a length of at least 70 mm along the top edge of the display ground. To achieve a smaller size of the internal LTE/WWAN antenna for mobile devices remains a challenging task, owing to the very limited available space therein. This design issue is even more challenging in the tablet or laptop computers mainly because the system ground plane or the display ground is much larger compared to that of the mobile handset and generally, its chassis (ground plane) resonant mode cannot be generated to aid in enhancing the bandwidths of the antenna [5–12].

In this article, we present a promising design of the internal tablet computer antenna using the combined techniques of using a coupling feed and a band-stop matching circuit to cover the LTE/WWAN operation with a decreased antenna size. The antenna is a coupled-fed loop antenna [13] that operates at its quarter-wavelength mode as the lowest resonant mode [14, 15] and can provide two wide operating bands (704–960 and 1710–2690 MHz) to cover the eight-band LTE/WWAN operation (LTE700/GSM850/900 and GSM1800/1900/UMTS/LTE2300/2500 bands).

The use of a band-stop matching circuit which generally does not increase the occupied volume of the antenna and generates a parallel resonance [16] at about 1200 MHz, which results in a new resonance (zero reactance) occurred nearby and leads to a new resonant mode excited at about 950 MHz. This new resonant mode greatly enhances the bandwidth of the antenna's lower band and combines the quarter-wavelength mode of the coupled-fed loop antenna to cover the desired LTE700/GSM850/900 operation. The antenna's upper band is formed by the higher order resonant modes of the coupled-fed loop antenna and an additional resonant mode contributed by the coupling feed, which is a T-shape strip in the proposed design. The upper band shows a wide bandwidth of larger than 1 GHz to cover the desired GSM1800/1900/UMTS/LTE2300/2500 operation.

Owing to the proposed techniques of using a coupling feed and a band-stop matching circuit, the antenna requires a length of 55 mm along the top edge of the display ground of the tablet computer only. The antenna's metal pattern includes a printed pattern which can be disposed on a thin FR4 substrate of planar size 10 × 55 mm^2, and a metal strip of size 4 × 55 mm^2 which is connected orthogonally to the printed pattern on the substrate to form a part of the antenna's loop pattern. With comparison to the reported internal LTE/WWAN antenna for the tablet or laptop computers [1–4], the proposed antenna shows a smallest occupied volume for covering the LTE/WWAN operation. In this article, details of the proposed antenna are described. Effects of the coupling feed and the band-stop matching circuit for bandwidth enhancement of the proposed antenna are discussed.

2. PROPOSED ANTENNA

Figure 1 shows the geometry of the proposed LTE/WWAN coupled-fed loop antenna with a band-stop matching circuit. The loop antenna comprises a T-shape radiating feed, a coupled shorted strip, an antenna ground, and a band-stop matching circuit on the antenna ground. The antenna is mainly disposed on a